Multi-rotor Wind Farm Layout Optimization

Multi-rotor Wind Farm Layout Optimization

Nicolas Kirchner-Bossi and Fernando Porté-Agel

Wind Engineering and Renewable Energy Laboratory (WiRE), École Polytechnique Fedérale de Lausanne (EPFL), CH-1015 Lausanne, Switzerland.

E-mail: nicolas.kirchnerbossi@epfl.ch

Abstract.

Multi-rotor wind turbines have shown a faster wake recovery than equivalent single-rotor turbines. In this work the potential benefit of a wind farm with multi-rotor turbines is assessed through the optimization of the turbine positions using the CEGA wind farm optimization algorithm, for different power densities. The EPFL analytical wake model is used to compute the power output at each turbine. The wake growth rate in this model depends on the incoming turbulence intensity. However, added turbulence intensities caused by multi-rotors affecting downstream turbines in a wind farm have recently been shown to be different from those by single-rotors. Here, two simple expressions are derived, one for the added turbulence intensity behind a multi-rotor and another for its relationship with the wake growth rate in a downstream turbine. Results on fixed layouts show multi-rotor power output improvements between 6% (3D spacings) and 0.3% (10D spacings). This benefit is bigger under relatively low ambient turbulent levels. The optimization of a full-scale wind farm layout (Horns Rev, 80-turbines) using multi-rotors provides an advantage of 0.66% and 0.79% against the optimized and the baseline single-rotor layouts, respectively. Optimizations of power densities with average inter-turbine distances of 4D and 10D show 2.75% and 0.1% improvements, respectively.

1. Introduction

Multi-rotor (MR) wind turbines present certain features that could potentially lead to performance improvement in a wind farm, compared to single-rotor (SR) turbines. One of the most important is the faster wake recovery compared to single-rotor turbines with similar overall rated power and rotor area, as shown in several recent large-eddy simulation (LES) studies [1–5]. This feature can result in bigger power output values for downstream turbines in a wind farm, as shown in different cases considering aligned turbine rows [1, 5] or staggered turbines [4].

Other positive aspects of a multi-rotor wind turbine rely on the general agreement that their produced streamwise added turbulence intensity is smaller than equivalent single-rotor turbines (especially for distances ≥ 3 equivalent single-rotor diameters), which might lead to smaller fatigue loads on downstream turbines. Finally, they could provide an alternative to the current trend of increasing turbine size, which can become especially challenging beyond 10MW [6].

The aim of this work is to investigate the potential added value of a multi-rotor wind farm in terms of its overall power output, compared to an equivalent single-rotor wind farm. One strategy designed to explore and expand the limits of the efficiency in a wind farm is the optimization of the positions of its turbines. During the last two decades, multiple studies have worked in this line of wind farm layout optimization (WFLO) [7], showing that the performance

of the wind farm can be improved from different aspects. Although the most considered aspect is the wind power production [8–11] WFLO has been also addressed from other perspectives, considering other cost functions, such as the level of noise [12, 13] or the economical cost (e.g., [14, 15]). Hence, applying a WFLO strategy can be an appropriate way to obtain a more clear picture of the real potential benefits of a multi-rotor wind farm compared to a single-rotor one. Naturally, before directly addressing the optimization of the turbine positions, other questions of interest can be addressed. In this way, investigating the sensitivity to the power density in a wind farm composed of multi-rotors, and especially in comparison to the single-rotor case, is a task that has not been addressed yet.

Multiple contributions have shown that a convenient way to carry out a WFLO strategy consists of using an analytical model that represents the turbine wake not only in an accurate, but also in a fast manner, so that multiple (thousands) of possible layouts can be assessed in a reasonable computation time and thus be competitive in the search of an optimal solution (see review from [7] and references therein). Among the existing analytical wake models (e.g., [16–18]), the EPFL analytical wake model [18, 19] has shown good accuracy in the turbine wake representation against LES and wind tunnel measurements compared to other approaches. The usage of an analytical wake model in WFLO has proven to provide best results when carried out in combination with some metaheuristic algorithm (generally Genetic Algorithms [8, 11]), but also others as such as Particle Swarm Optimization [20] or random search [9].

Notwithstanding all this, to be in condition to apply an analytical wake model such as the EPFL one on multi-rotor turbines, some validations are required first. Firstly, some parameters of the EPFL model related to the growth of the wake have been shown to be variable and strongly related to the turbulence intensity affecting the turbine [19]. This poses the immediate question of whether the same relationship between the growth rate and the ambient turbulence used for single-rotor turbines is also valid for multi-rotor turbines, or if it needs to be modified. Secondly, and precisely for that reason, a proper expression for the added turbulence intensity in the multi-rotor turbine becomes necessary. This would allow defining the turbulence intensity values affecting downstream turbines in the wind farm in a similar way as in the single-rotor case, for which different empirical expressions have been proposed (e.g., [21, 22]). This is especially relevant following the differences evidenced by [2, 3] between the added turbulence behind a multi-rotor compared to a single-rotor. In this work these two issues are addressed.

2. Multi-rotor and Single-rotor wind turbine models

The turbines considered in this work are the 4R-V29 and the V58 turbines from [3], which hereafter will be referred to as the multi-rotor (MR) and single-rotor (SR) turbines. 4R-V29 is a 225kW 4-rotor turbine composed of 4 Vestas-V29, arranged as shown in Fig. 1, with rotor diameters of d=29.2m at hub heights of 29.04m and 59.50m for the lower and the upper pair of rotors, respectively. The 4R-V29 is the only multi-rotor wind turbine to have been tested at full scale in the field. In turn, the V58 turbine is an equivalent, theoretical single-rotor turbine, with a similar area as the 4R-V29 (thus with diameter D=2d), and a rated power of 900kW, four times the one of the V29s. Its hub height is placed in the center of the 4R-V29 turbine, i.e., at 44.27m. The V29 power curve was extracted from its manufacturer, and that for the V58 was set to four times the V29 one. Finally, the power alterations due to the effects of the 4-rotor interaction found out in [3] were included in the multi-rotor power curve.

3. The EPFL Gaussian wake model

Analytical models of the velocity deficit behind a turbine are useful when thousands of different layouts under multiple wind flow regimes need to be evaluated, as in the case of a realistic wind farm layout optimization (WFLO) framework. Due to its demonstrated accuracy to reproduce the wake of a wind turbine with respect to other approaches, we considered the EPFL Gaussian

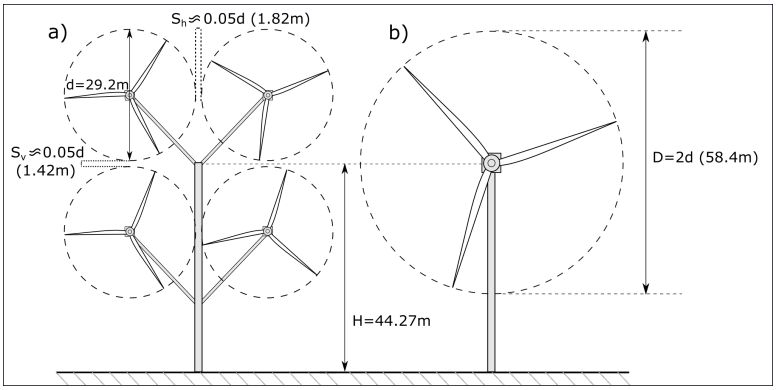

Figure 1. Scheme of the MR 4R-V29 (a) and the SR V58 (b).

model [18], alongside with the linear wake aggregation proposed by [19]. The EPFL Gaussian wake model can be defined in terms of the wake velocity deficit ΔU, as follows:

$$\Delta U = U_\infty \left(1 - \sqrt{1 - \frac{C_t}{8(k^* x/d_0 + \varepsilon)^2}}\right) \times exp\left(-\frac{1}{2(k^* x/d_0 + \varepsilon)^2}\left\{\left(\frac{z - z_h}{d_0}\right)^2 + \left(\frac{y}{d_0}\right)^2\right\}\right), \quad (1)$$

where U_∞ represents the undisturbed wind velocity, C_t the turbine thrust coefficient, x, y and z are the streamwise, spanwise and vertical coordinates, respectively, z_h is the hub height, d_0 the rotor diameter, k^* represents the wake expansion rate and ε stands for the initial wake growth. ε can be defined as [18]:

$$\varepsilon = C_\varepsilon \sqrt{\frac{1-a}{1-2a}} \quad (2)$$

where a is the turbine induction factor and C_ε a tunable parameter. [18] obtained C_ε values between 0.18 and 0.2 for SR after linear fits, whereas [1] assigned values of 0.18 and 0.2 for MR and SR turbines respectively.

4. A model for the turbulence behind a multi-rotor turbine

To date several empirical models for the added turbulence intensity (I^+) caused by the SR turbine have been proposed [21, 22], and have been used successfully in combination with analytical wake modeling [11, 19]. Specifically, [19] established a linear relationship between the turbulence affecting the turbine and its wake growth rate k* (EPFL wake model) being produced downstream. However, the different behavior of I^+ in a MR compared to the SR case is well known, with higher levels for MR up to a few D_{eq} distances (2-4) and lower levels than SR beyond that point [2, 3]. Due to these differences, in this work a specific model for the added turbulence behind the MR turbine has been derived. This has been done through an empirical non-linear fit to RANS results (hereafter I-RANS) on a multi-rotor turbine [3], which provides added turbulence values for three different total ambient turbulence intensity $I_{t,\infty}$ amounts, 0.05, 0.10 and 0.20. I-RANS turbulence values (and thus the model) are expressed in terms of the total, rotor disk-averaged, direct subtracted turbulence I^+_{ds} between the disk-averaged turbulence in the wake I, and the incident turbulence $I_{t,\infty}$, so $I^+_{t,ds} = I_t$ - $I_{t,\infty}$. A Levenberg-Marquardt least-squares fit was carried out by parameterizing a general multiplying coefficient and exponential terms on the downstream distance and the ambient turbulence level, similarly to previous empirical expressions applied to SR [21, 22]. Additionally, a term related to the

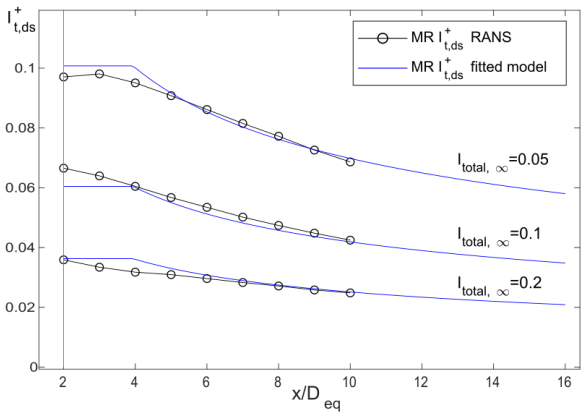

Figure 2. Total added turbulence intensity ($I_t - I_{t,\infty}$) profiles behind the turbine, according to the RANS data from [3] (white circles), and to the fitted model (blue), for different values of total incident turbulence ($I_{t,\infty}$=0.05, $I_{t,\infty}$=0.10 and $I_{t,\infty}$=0.20).

thrust coefficient (in this case in terms of the induction factor a) was extracted from [22]. The obtained model for $I^+_{t,ds}$ can be expressed in the following expression:

$$I^+_{t,ds} = 0.0559 \cdot a^{0.8325} \cdot I_{t,\infty}^{-0.7364} \cdot (x/D_{eq})^{-0.3936} \tag{3}$$

Due to the different behavior in the first part of the wake, a second expression was derived for distances $2 < D_{eq} < 4$, this time independent of the downstream distance:

$$I^+_{t,ds} = 0.0324 \cdot a^{0.8325} \cdot I_{t,\infty}^{-0.7364} \tag{4}$$

Figure 2 depicts the I-RANS dataset and the corresponding modeled I^+_{ds} for the three cases of $I_{t,\infty}$ (0.05, 0.1 and 0.2).

After obtaining a value of $I^+_{t,ds}$, it can be transformed to its more widely employed expression relying on the squared root difference between I_t and $I_{t,\infty}$ instead of its direct difference, so that

$$I_t^+ = \sqrt{{I_t}^2 - I_{t,\infty}^2} = \sqrt{(I^+_{t,ds} + I_{t,\infty})^2 - I_{t,\infty}^2} \ . \tag{5}$$

In addition, assuming a certain turbulence scheme that establishes a given relationship between the standard deviation of the streamwise velocity σ_u and the other two components (σ_v, σ_w), an expression for the streamwise turbulence intensity I_u can be derived. In this work it has been done by adopting the ratios from [23], for which σ_v/σ_u=0.8 and σ_w/σ_u=0.5, so the streamwise turbulence intensity can be defined as:

$$I_u = I_t \sqrt{\frac{3}{(1 + 0.8^2 + 0.5^2)}} \approx 1.26 I_t \ . \tag{6}$$

5. EPFL Gaussian wake model validation for multi-rotor wind farms

The linear positive relationship of the wake growth rate k^* in a SR and the turbulent intensity affecting it established by [19] allowed the appropriate usage of the EPFL Gaussian wake model in a SR wind farm, where downstream turbines are affected by turbulence intensity levels that differ from the ambient one (I_∞). Following the SR case, understanding how the wake growth rate k^* in a MR is linked to the turbulence intensity level affecting it is necessary in order to use the EPFL wake model within a MR wind farm appropriately. In addition, following [1, 5], the initial wake expansion C_ε can also be particularized. The specification for the k^*(I)

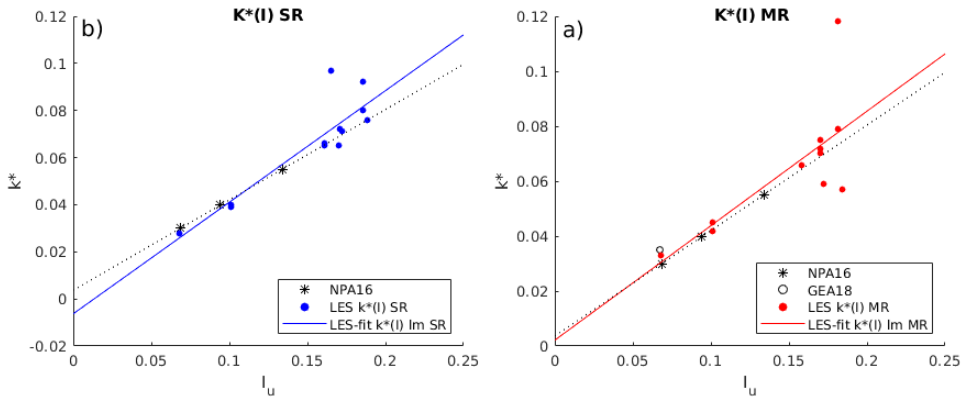

Figure 3. Resulting pairs of (k^*,I) data matching the LES power output profile from [4] using the EPFL Gaussian model, SR (a) and MR (b). Solid lines represent the linear fits from the the (k^*,I) pairs. Asterisks and black dotted line stand for the k^*(I) model from [19], whereas white circle represents the (k^*,I) point used by [1].

relationship and the C_ε can be done by using a MR wind farm dataset that details the velocity or the relative power in each turbine, the distances between them and the ambient turbulence intensity I_∞ (total or streamwise). This is the case for the LES-based power output profiles for 5 aligned turbines (hereafter LES-5T) from [4] ($5D_{eq}$ turbine distances) and [5] ($4D_{eq}$ and $6D_{eq}$ turbine distances), which motivated its usage in this work. These contributions apply a $I_{t,\infty}$=0.054 and 0.08, respectively, whereas both consider a turbine thrust coefficient C_t=0.75. The (k^*,I) relationship was addressed in terms of the streamwise turbulence intensity $I_{u,\infty}$, which was derived from the total value $I_{t,\infty}$ applying the scheme from [23] (Eq. 6). To assess the (k^*,I) relationship, first of all the turbulence intensity at each MR turbine is obtained by using eq. (3) and (4). To obtain the corresponding values for k^* at each turbine, a coordinate descent [24] optimization routine was applied in the streamwise direction. The algorithm works by defining the value of k^*_n at turbine n that allows reproducing the power output registered in turbine $n+1$, relying on the basis that k^*_n at turbine n modifies the downstream velocity (see eq. 1 for the EPFL wake model). Once k^*_n is fixed, k^*_{n+1} is subsequently defined according to the power value at turbine $n+2$, etc. This allows finally fixing N-1 values of k^*, N being the number of turbines in the wind farm. The routine was applied for a range of C_ε values (0.12-0.25) around the initial one (0.2) proposed by [18]. Assuming the linear k^*(I) relationship shown by [19, 25], we selected the C_ε case that provided the best goodness of fit, on the basis of both Pearson correlation r of the linear fit, and the average RMSE in the power prediction.

The linear k^*(I) model for SR in [19] was carried out for the specific case of C_t=0.8 (different than the LES-5T C_t=0.75). The fact that analytical wake models are highly sensitive to the turbine thrust [16, 18], motivated the derivation of a k^*(I) model also for SR, this time under the C_t LES-5T conditions. For the SR case we used the added turbulence expression proposed in [22] (hereafter I-Crespo), as previously done with the EPFL wake expression for SR wind farm modeling [11, 25].

Figure 3 shows the obtained (k^*,I) values, for SR (a) and MR (b), and their corresponding linear fits. Regarding SR, the most accurate results were obtained for a C_ε value of 0.174, which lies within the range of corresponding ε values shown in [18] and is close to the 0.2 value used in [19]. In general, results are in good agreement with those found by [18, 19] from LES data [26]. Wake growth rates k^* of the first turbines appeared slightly smaller than the corresponding figures for the C_t=0.8 model, which is consistent with a slightly smaller thrust coefficient. Although the value of the slope is near to that in [19], the higher value in the current

model might be explained by the fact that the (k^*,I) pairs in [19] are based exclusively in turbines exposed to undisturbed flow, whereas in the current work downstream turbines are considered in addition to exposed to undisturbed flow, something that might involve a different relationship between k^* and I. Regarding MR, the best fit was attained for a C_ε=0.151, slightly smaller than the SR value. A similar relationship between SR and MR values for C_ε was obtained by [1], with a value of 0.18 and 0.2 for the MR and SR cases, respectively. In this case, k^* values are slightly above the [19] model, matching very well the (k^*,I) values used in [1]. Although some points provided a relatively big residual value in the linear fit, still a rather favorable goodness of fit was obtained, with r=0.74.

Following, the obtained linear expressions are detailed:

$$k^*_{SR,Ct0.75}(I_u) = -0.0063 + 0.4737 I_u, \tag{7}$$

$$k^*_{MR,Ct0.75}(I_u) = 0.0021 + 0.4168 I_u \ . \tag{8}$$

Given the features of the LES-5T dataset and the obtained downstream turbulence values, these expressions are restricted to a streamwise turbulence intensity range of $0.068 < \mathrm{I}_u < 0.2$.

Applying the EPFL wake model with the obtained k^*(I) expressions and the calibrated C_ε values provided an average power estimation error of 2.52% and 2.45% with respect to the relative power in the LES-5T dataset, respectively for SR and MR (the first turbine is not considered in the error computation as its value is always 1).

Figure 4.a shows the power output profiles for different rows of 10 wind turbines for inter-turbine spacings between $4D_{eq}$ and $11D_{eq}$, for both the SR and MR cases, obtained through the EPFL wake model calibrated for SR and MR, as well as the data from LES-5T ($4D_{eq}$, $5D_{eq}$ and $6D_{eq}$). Ambient turbulence intensity levels were alternately set, in order to match those in LES-5T. Results on the different rows reflect higher power values for the MR ones for the first downstream turbines (generally the 2nd and 3rd turbines) compared to the SR turbines, as previously reported by [4, 5]. This behavior is more pronounced for smaller inter-turbine distances and ambient turbulence levels. After the first 3 to 4 turbines, power values tend to stabilize around a similar value, which is slightly smaller for the MR case, a circumstance also seen in LES results [5]. These effects can be more clearly seen in figure 4.b, which shows the ratio of the overall power output between MR and SR, with respect to an increasing amount of turbines considered in a row, and their inter-turbine distance, for the two $\mathrm{I}_{t,\infty}$ values considered. Results show the overall power output ratio between MR and SR (PO_{MR} / PO_{SR}) to be sensitive to the ambient turbulence intensity $\mathrm{I}_{t,\infty}$, with negative (positive) values in most of the configurations where a value of $\mathrm{I}_{t,\infty} = 0.08$ ($\mathrm{I}_{t,\infty} = 0.054$) is applied. However, considering each configuration case by case, MR increases are considerably bigger than the SR ones in both turbulence regimes, with maximum ratios of 10% ($\mathrm{I}_{t,\infty}$=0.08) and 17% ($\mathrm{I}_{t,\infty}$=0.054) and minimum ones of −4% ($\mathrm{I}_{t,\infty}$=0.08) and −0.6% ($\mathrm{I}_{t,\infty}$=0.054).

6. Application to a real wind farm and power density optimization

After assessing the EPFL wake model calibrated for the MR and SR cases on different 10-turbine rows, it was applied to a real wind farm case-study in order to investigate the different performances for the MR case concerning the SR case, from different aspects such as the effects of partial wakes and the power density. To do this we considered the wind farm layout of Horns Rev I (HR) wind farm, a wind farm with 80 Vestas V-80 located in the North Sea, 12 km off the Danish coast [27], with inter-turbine distances equal to 7D. To keep the same relative inter-turbine distances, turbine positions were set to $7D_{eq}$ distances in this work.

The potential effects of partial wakes were studied by applying the EPFL wake model to the HR layout for all wind directions, with an angular resolution of 1 deg., and fixed incoming wind velocity U_0 of 10 m/s, for both SR and MR cases. Results (fig. 5.a) showed that a partial

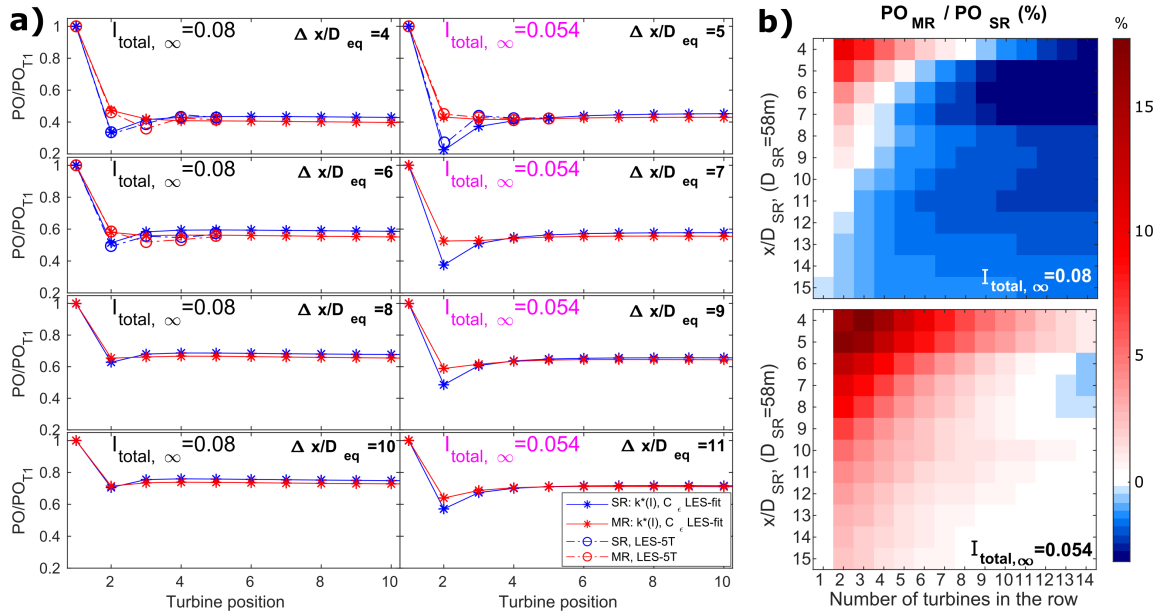

Figure 4. (a) Power output of the HR 10-turbine row for a westerly wind velocity, relative to the first turbine, for different inter-turbine distances D_{eq} and two $I_{total,\infty}$ (0.08 and 0.054). Solid lines show the LES-based model, for MR (red) and SR (blue), as circle-dashed lines stand for the LES-5T data (in 4D, 5D and 6D). (b) Overall power output ratio between MR and SR (PO_{MR}/PO_{SR}) according to the normalized inter-turbine distances and the amount of aligned turbines, for the two $I_{total,\infty}$ considered, for $4 < \Delta x/D \leq 15$ and $1 < N \leq 14$.

wake environment, more realistic than the perfectly aligned one, is generally beneficial for a MR wind farm configuration, even for a high ambient turbulence level. In this way, bigger power outputs than the SR case were obtained for most wind directions, leaving a SR advantage nearly exclusively in the perfectly aligned cases. As a result, even though the overall power output was bigger for the SR case within the $7D_{eq}$ 10-turbine row ($I_{t,\infty}$=0.08 case, fig. 4.b), when considering all directions MR power output becomes bigger for the two $I_{t,\infty}$ values.

In order to analyze the effect of the power density in the performance of the MR turbine wind farm compared to the SR one, the power output for all wind directions was assessed for the Horns Rev layout considering inter-turbine distances other than $7D_{eq}$, this implying bigger power densities for smaller distances. After applying this procedure to HR layouts with inter-turbine distances between $3D_{eq}$ and $10D_{eq}$, MR showed bigger overall (considering all directions) power output values for all inter-turbine distances (fig. 5.b). Specifically, the benefit of MR with respect to SR considering both turbulence levels (0.08 and 0.054) showed to be positively related to the power density, from average MR power performance improvements of 0.2% for the 10_{eq} case up to 6% for the $3D_{eq}$ case.

7. Wind farm layout optimization

In the last step of this work, the layout optimization for a realistic wind farm framework was addressed, for both MR and SR cases, on the basis of the Horns Rev wind farm. For these optimizations, the Crossover-elitist Genetic Algorithm (CEGA) from [11], an ad-hoc WFLO Genetic Algorithm (GA) was used, as it showed higher optimization performance compared to other strategies on similar conditions. During the GA optimization, wind power for each potential solution was assessed on 72 different wind directions (i.e., angular resol. of 5 deg.).

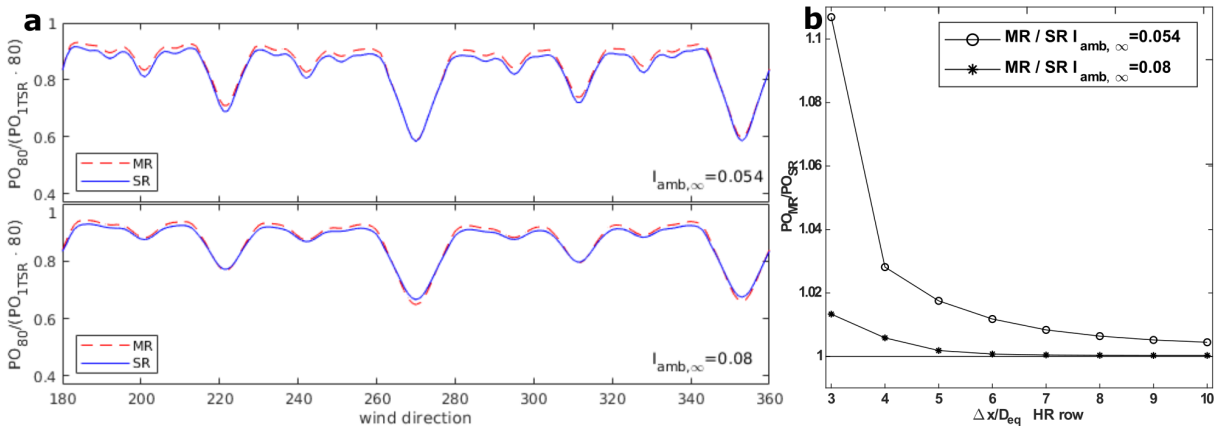

Figure 5. a) Wind power output for the Horns Rev relative ($7D_{eq}$) baseline layout for wind directions from south to north, (1-deg. angular resol.), for the for the MR (red) and the SR (blue) cases, relative to 80 SR turbines exposed to free-stream, and for $I_{total,\infty}$ of 0.054 (above) and 0.08 (below). (b) Ratio between the overall power output for MR and that for SR, for $I_{total,\infty}$=0.054 (circled line) and 0.08 (asterisk line), considering the real wind direction frequencies at Horns Rev.

A termination condition for the evolution was set to 2000 generations. After the evolution, an evaluation with 120 wind directions (3 deg. resol.) was applied. To be consistent with the obtained K^*(I) models, the optimization was limited to a constant C_t on all turbines. An incoming hub height free stream velocity of 10 m/s and an ambient total turbulence intensity of 0.06 (inside the range of the two LES-5T values) were imposed. A corresponding weight was associated to each wind direction according to their frequencies from Horns Rev measurements [27]. Due to the fact that the EPFL wake model is not defined in the near wake [18, 19], a minimum distance constraint between turbines of 3 real diameters was imposed (i.e., $3D_{eq}$ and $1.5D_{eq}$ for SR and MR, resp.). Previous studies [9–11] have shown that this constraint is not involved in the optimized layouts, as turbines meet a low performance within that distance. Finally, the translation of the rotor centers in the MR turbine produced by oblique wind directions can imply a reduction in the relative distance between rotors from two MR turbines. To prevent this effect, the minimum distance constraint for MR turbines was increased from $1.5D_{eq}$ to $2D_{eq}$.

The optimized layouts for the Horns Rev wind farm are shown in figure 6. As previously observed in [11], the SR wind farm shows a wide space after the perimeter turbines, especially on the left edge, where most prevalent wind directions occur. This effect is reduced in the MR case, due to the smaller observed power decrease in the second MR turbine. Results on the power output showed an improvement with respect to the optimized SR case of 0.66%, an improvement that turns into 0.79% if the comparison is done against the Horns Rev baseline (SR).

In order to investigate the sensitivity of the optimization potential to the power density and to the problem dimensionality, smaller wind farms with areas were optimized for different power densities (PD). This smaller area was set proportional to 20 turbines of the Horns Rev 1 baseline layout, 5 in the x-axis by 4 in the y-axis. In this way, PDs were established according to this regular grid, but with inter-turbine distances of $4D_{eq}$, $7D_{eq}$ and $10D_{eq}$ (hereafter $PD_{4D_{eq}}$, $PD_{7D_{eq}}$ and $PD_{10D_{eq}}$) with 20 turbines, for both MR and SR cases.

Results showed a power improvement of 2.76% for the $PD_{4D_{eq}}$ case, whereas rather similar values compared to SR were obtained for the other two cases. As it can be observed, the $PD_{4D_{eq}}$ MR case shows half the turbines than SR in the inner part of the wind farm. This can be due, on

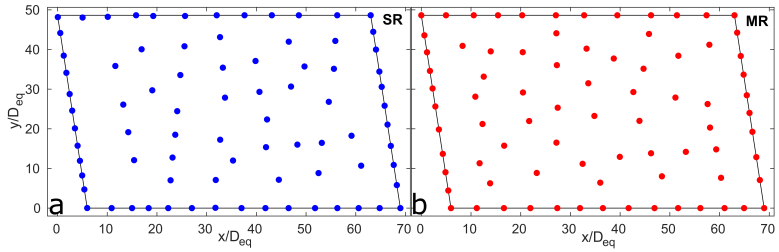

Figure 6. Optimized layouts for the single-rotor (a) and the multi-rotor (b) wind farms for the extended wind farm (80T).

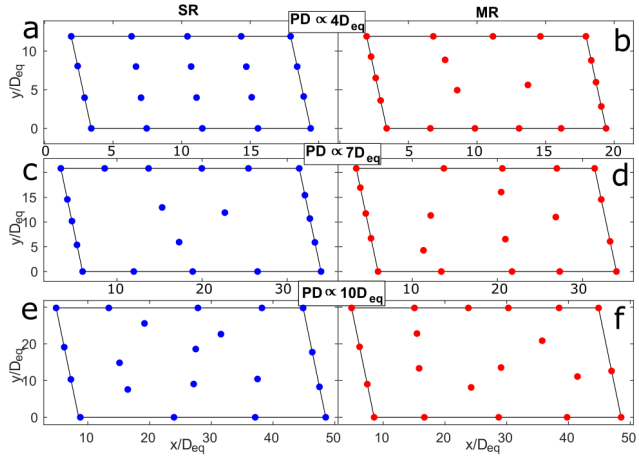

Figure 7. Optimized layouts for the Single-rotor (a,c,e) and the Multi-rotor (b,d,f) reduced wind farms (20T), for a power density equivalent to an average distance of $4D_{eq}$ (a,b), $7D_{eq}$ (c,d) and $10D_{eq}$ (e,f).

one side, to MR having (in absolute terms) a smaller minimum inter-turbine distance constraint (3d=1.5D_{eq}) compared to SR (3D_{eq}), which allows turbine positions not allowed in SR on one side, and, on the other, to the fact of MR having a faster wake recovery. This pattern of more turbines in the inner wind farm for MR is no longer clear for the other two PD cases, partly due to larger degrees of freedom in the SR turbines. The reason for not improving the performance in the $PD_{7D_{eq}}$ and $PD_{10D_{eq}}$ cases remains unclear. However, the fact that a 0.79% improvement is obtained in the 80-turbine optimization (also with a $PD_{7D_{eq}}$) suggests that the capacity of improvement for the MR case is associated with the problem dimensionality.

8. Conclusions

In this work the potential benefits of a wind farm with multi-rotor turbines compared to a single-rotor one has been investigated from different aspects, including its layout optimization in an extensive problem (80 turbines). This has been done by means of the EPFL analytical wake model[18, 19], which has been calibrated and validated using LES data [4, 5] for the specific case of a turbine thrust coefficient of 0.75.

The faster wake recovery of the multi-rotor wind turbine reported in several recent contributions [1–5] is observed to promote a higher power output performance in a wind farm, compared to the single-rotor case. This multi-rotor wind farm benefit is especially clear for high power densities (equivalent to a grid with $\simeq$4D inter-turbine distances). Although it is observed to decay as power density decreases, this advantage persists for smaller values (>10D equivalent

power densities). This is shown on 10-turbine aligned rows, gridded wind farm layouts and full wind farm optimization results.

The layout optimization from the full-scale wind farm (Horns Rev I[27], 80 turbines) provided a power output increase of 0.66% with respect to the optimized single-rotor wind farm, and 0.79% against the gridded baseline single-rotor layout. Layout optimization in a reduced scanrio (20 turbines) with bigger power densities (corresponding to $\simeq 4D_{eq}$) provided power output improvements of 2.76%.

This work is limited to the specific case of a turbine thrust coefficient of 0.75, and for a limited turbulence intensity range. This means that considering other (and more variable) conditions might make these results vary. Further work involving a strategy that allows applying the framework presented in this work straightforwardly on different C_ts could provide meaningful insights. Finally, carrying out further multi-rotor simulations and/or wind tunnel experiments on other incoming turbulence intensities and thrust coefficients could be highly valuable to complement the empirical expressions proposed in this work.

References

[1] Ghaisas N S, Ghate A S and Lele S K 2018 *Journal of Physics: Conference Series* vol 1037 (IOP Publishing) p 072021

[2] Bastankhah M and Abkar M 2019 *Physics of Fluids* **31** 085106

[3] van der Laan P, Andersen S J, García N R, Angelou N, Pirrung G, Ott S, Sjöholm M *et al.* 2019 *Wind Energy Science* **4** 251–271

[4] van der Laan M P and Abkar M 2019 *Journal of Physics: Conference Series* vol 1256 (IOP Publishing) p 012011

[5] Ghaisas N S, Ghate A S and Lele S K 2020 *Wind Energy Science* **5** 51–72

[6] Noyes C, Qin C and Loth E 2018 *Renewable energy* **116** 749–754

[7] Herbert-Acero J F, Probst O, Réthoré P E, Larsen G C and Castillo-Villar K K 2014 *Energies* **7** 6930–7016

[8] Mosetti G, Poloni C and Diviacco B 1994 *Journal of Wind Engineering and Industrial Aerodynamics* **51** 105–116

[9] Feng J and Shen W Z 2015 *Renewable Energy* **78** 182–192

[10] Gebraad P, Thomas J J, Ning A, Fleming P and Dykes K 2017 *Wind Energy* **20** 97–107

[11] Kirchner-Bossi N and Porté-Agel F 2018 *Energies* **11** 3268

[12] Sorkhabi S Y D, Romero D A, Beck J C and Amon C H 2018 *Renewable energy* **126** 341–353

[13] Mittal P, Mitra K and Kulkarni K 2017 *Energy conversion and management* **132** 147–160

[14] Rodrigues S, Bauer P and Bosman P A 2016 *Renewable and Sustainable Energy Reviews* **65** 587–609

[15] DuPont B and Cagan J 2016 *Optimization and Engineering* **17** 77–103

[16] Jensen N O 1983 *Risø National Laboratory Roskilde*

[17] Frandsen S, Barthelmie R, Pryor S, Rathmann O, Larsen S, Højstrup J and Thøgersen M 2006 *Wind Energy: An International Journal for Progress and Applications in Wind Power Conversion Technology* **9** 39–53

[18] Bastankhah M and Porté-Agel F 2014 *Renewable Energy* **70** 116–123

[19] Niayifar A and Porté-Agel F 2016 *Energies* **9** 741

[20] Rahmani R, Khairuddin A, Cherati S M and Pesaran H M 2010 *IPEC, 2010 Conference Proceedings* (IEEE) pp 134–139

[21] Quarton D and Ainslie J 1990 *Wind Engineering* 15–23

[22] Crespo A, Herna J *et al.* 1996 *Journal of wind engineering and industrial aerodynamics* **61** 71–85

[23] Panofsky H and JA D 1984 *Atmospheric Turbulence Models and Methods for Engineering Applications* (Wiley and Sons, New York)

[24] Luo Z Q and Tseng P 1992 *Journal of Optimization Theory and Applications* **72** 7–35

[25] Niayifar A and Porté-Agel F 2015 *Journal of physics: conference series* vol 625 (IOP Publishing) p 012039

[26] Wu Y T and Porté-Agel F 2012 *Energies* **5** 5340–5362

[27] Sommer A and Hansen K 2002 Wind resources at horns rev Tech. rep. Technical Report D-160949, Tech-wise